POLITECNICO DI TORINO
Repository ISTITUZIONALE

Anisotropic linear elastic properties of fractal-like composites

Original
Anisotropic linear elastic properties of fractal-like composites / Carpinteri, Alberto; Cornetti, Pietro; Pugno, Nicola; Sapora, ALBERTO GIUSEPPE. - In: PHYSICAL REVIEW E, STATISTICAL, NONLINEAR, AND SOFT MATTER PHYSICS. - ISSN 1539-3755. - 82, 056114:(2010), pp. 1-7. [10.1103/PhysRevE.82.056114]

Availability:
This version is available at: 11583/2379962 since: 2016-05-13T10:02:22Z

Publisher:
AMER PHYSICAL SOC, ONE PHYSICS ELLIPSE, COLLEGE PK, MD 20740-3844 USA

Published
DOI:10.1103/PhysRevE.82.056114

Terms of use:

This article is made available under terms and conditions as specified in the corresponding bibliographic description in the repository

Publisher copyright

(Article begins on next page)

12 October 2024

Anisotropic linear elastic properties of fractal-like composites

Alberto Carpinteri, Pietro Cornetti, Nicola Pugno, and Alberto Sapora*
Department of Structural Engineering and Geotechnics, Politecnico di Torino, Corso Duca degli Abruzzi 24, 10129 Torino, Italy
(Received 15 April 2010; revised manuscript received 8 July 2010; published 16 November 2010)

In this work, the anisotropic linear elastic properties of two-phase composite materials, made up of square inclusions embedded in a matrix, are investigated. The inclusions present a fractal hierarchical distribution and are supposed to have the same Poisson's ratio as the matrix but a different Young's modulus. The effective elastic moduli of the medium are computed at each fractal iteration by coupling a position-space renormalization-group technique with a finite element analysis. The study allows to obtain and generalize some fundamental properties of fractal composite materials.

DOI: 10.1103/PhysRevE.82.056114 PACS number(s): 62.20.F−, 61.43.Hv, 05.45.Df

I. INTRODUCTION

The determination of the effective linear elastic properties of multihipase materials has been the object of several studies in the last decade. Indeed, understanding how the macroscopic mechanical properties of a material are related to its microstructure emerges as a primary concern since it may provide guidance to the synthesis of new materials with specific properties.

Most of the related works presented in the paper refer to two-phase isotropic composites, where circular (or spherical, in the case of a three-dimensional analysis) inclusions, overlapping or not, are embedded in a matrix of a different phase. A brief résumé on the main recent approaches is herein presented. A numerical technique combining digital-image and spring network schemes was developed in [1] to determine the effective moduli of a sheet containing circular inclusions or holes. The algorithm was later extended to study two- and three-dimensional composites with equal Poisson's ratio between the phases [2,3]. Through the Cherkaev-Lurie-Milton theorem [4], the problem was also faced analytically by Thorpe and Jasiuk [5], while semianalytical studies, in the high concentration limit, were carried out by Zimmerman [6], applying the Mori-Tanaka [7] method and effective medium theories [8,9]. An interesting review on all these approaches can be found in [10]. More recently, a mathematical approach based on the complex-value Kolosov-Muskhelishvili potential was put forward in [11] to investigate the Poisson's ratio of planar composites.

The main results related to the works cited above show that the effective Young's modulus E of isotropic porous materials is independent of the Poisson's ratio of the solid phase υ_h in two dimensions and mildly dependent in three dimensions over the specific range $0 \leq \upsilon_h \leq 0.5$ [12]. Moreover, as the solid fraction decreases to the percolation threshold, the effective Poisson's ratio υ converges to a fixed point $\bar{\upsilon}$, independent of υ_h. In the specific case where the phases are solid and possess the same Poisson's ratio, there always exists a critical value $\upsilon^* = \bar{\upsilon}$, which results to be independent of the inclusion fraction ρ. The predicted value for $\bar{\upsilon}$, as well as that of the percolation threshold, depend on the shape of inclusions [13–16]. For two or three dimensional materials containing circular or spherical inclusions, for instance, the percolation threshold is nearly equal to 2/3 or 1 (i.e., 100% porosity), respectively, and υ tends toward the value $1/(2d-1)$, d being the dimension [1–6].

Little attention has been paid, so far, to the composite microstructure, which often shows a multiscale behavior, being formed over a wide range of length scales [2]. Since natural optimization suggests self-similarity [17,18], the possibility of analyzing the mechanical properties of multiscale materials by means of a fractal approach has been widely accepted by the scientific community [19–22]. Elastic properties of fractal structures have been generally investigated by considering them as spring-based systems of isotropic percolation clusters [23–33] or the Sierpinski gasket [34,35]. The two independent Lamé coefficients, which describe their elastic response, are found to possess the same power-law scaling, as long as the size of the system is less than the correlation length. A power-law behavior, albeit with different scaling exponents, is detected also for the moduli related to superelastic percolation networks [28,32], where a fraction of the springs are totally rigid and the rest are soft, and for other material properties, such as transport (see, for instance, [28,30,32,36,37] and related references) and failure ones [26,31,32]. Eventually, it is worthwhile mentioning the recent works by Latva-Kokko *et al.* [38,39] and by Head *et al.* [40], who studied two-dimensional flexible rod networks and showed that, differently from the geometric quantities describing the fractal structure of the percolating cluster, the mechanical properties at the rigidity percolation transition are distinct from previously investigated lattice schemes.

In spite of this, only few approaches have been proposed to evaluate the effective elastic moduli of fractal composites in the framework of continuum mechanics hitherto. The porous Sierpinski carpet, considered as the archetype of bidimensional fractal structures, was first investigated, from a mechanical point of view, by Sheng and Tao [41]. Based on the iterative solution of the Dyson equation for elastic wave scattering in inhomogeneous media, the independent components of the elastic modulus tensor were evaluated for the first three fractal iterations, showing a different scaling behavior. Analogous results were successively obtained by Poutet *et al.* [42], by adopting a multiple scale technique. The same procedure was applied also to study other fractal

*Corresponding author. FAX: +39 011 090 4899; alberto.sapora@polito.it

 ©2010 The American Physical Society

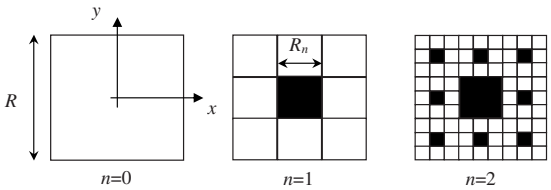

FIG. 1. First two iterations of a Sierpinski carpet: black squares represent the inclusions.

media, such as the Menger sponge or the fractal foam. On the other hand, Oshmyan *et al.* [43] showed, by coupling a position-space renormalization group (PSRG) technique [25,30] with a finite element (FE) analysis, that this behavior is limited only to the initial fractal generations: the effective elastic moduli asymptotically approach the same power-law behavior. This result holds for both infinitely soft or rigid inclusions although with a different scaling exponent. Similar conclusions were also recovered by Dyskin [21], through a self-consistent method, and by Novikov and co-workers, who developed an iterative averaging method to derive the elastic [44] and the conductivity [45] properties of inhomogeneous media with chaotic structure.

In the present work, the PSRG technique is exploited to study how the stiffness ratio between the phases affects the elastic properties of a Sierpinski carpet where both phases have the same Poisson's ratio. Although the linear elastic behavior of each phase is modeled as isotropic, the effective general response of the composite is anisotropic. As the number of fractal iterations increases, the inclusion concentration increases, and both the coefficient of anisotropy and the Poisson's ratio present a stationary point. Their values are found to depend on the constant of proportionality, i.e., on how stiffer or softer the inclusions are with respect to the matrix. Furthermore, in the limit cases, i.e., voids and infinitely rigid inclusions, these points become fixed, resulting independent of the host elastic moduli [43].

II. CONSTITUTIVE RELATIONSHIP AND NUMERICAL PROCEDURE

The stress-strain relationship $\{\sigma\}=[H]\{\varepsilon\}$ of a square symmetric material, in plane stress conditions, reads as

$$\begin{Bmatrix} \sigma_x \\ \sigma_y \\ \tau_{xy} \end{Bmatrix} = \begin{bmatrix} H_{11} & H_{12} & 0 \\ H_{12} & H_{11} & 0 \\ 0 & 0 & H_{33} \end{bmatrix} \begin{Bmatrix} \varepsilon_x \\ \varepsilon_y \\ \gamma_{xy} \end{Bmatrix}, \tag{1}$$

where the three independent coefficients H_{11}, H_{12}, and H_{33} of the stiffness matrix $[H]$ are sufficient to describe the elastic properties of the structure. This is the case of the Sierpinski carpet when the material symmetric axes coincide with the reference system xy (Fig. 1). By denoting with $\Omega^{(n)}$ the area occupied at the nth generation of the carpet, the constitutive law

$$\{\sigma\}^{(n)} = [H]^{(n)}\{\varepsilon\}^{(n)} \tag{2}$$

provides the relationship between the mean stress $\{\sigma\}^{(n)}$ and the mean strain $\{\varepsilon\}^{(n)}$, where it is assumed that $(\cdot)^{(n)}=1/\Omega^{(n)}\int_{\Omega^{(n)}}(\cdot)dxdy$.

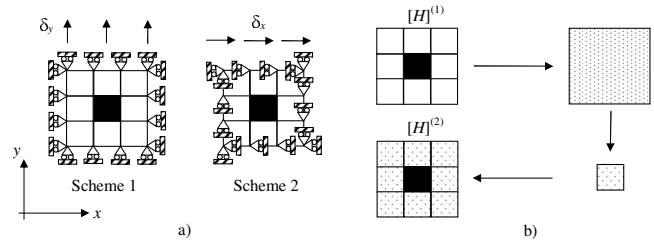

FIG. 2. (a) Different schemes adopted to evaluate the elastic coefficients of a Sierpinski carpet and (b) PSRG technique to pass from $[H]^{(1)}$ to $[H]^{(2)}$ using a first-order structural cell.

The effective elastic coefficients, at each fractal iteration n, can be calculated according to the two schemes displayed in Fig. 2(a). By indicating with δ_x and δ_y the two imposed displacements on the top side of the carpet in the direction of the axes x and y, respectively, and with R the characteristic side of the carpet (Fig. 1), it is possible to evaluate $H_{11}{}^{(n)}$ and $H_{12}{}^{(n)}$ from scheme 1:

$$H_{11}{}^{(n)} = F_y/\delta_y, \quad \text{where} \quad F_y = 2\int_0^{R/2} \sigma_y(x)dx, \tag{3a}$$

$$H_{12}{}^{(n)} = F_x/\delta_y, \quad \text{where} \quad F_x = 2\int_0^{R/2} \sigma_x(y)dy, \tag{3b}$$

and $H_{33}{}^{(n)}$ from scheme 2:

$$H_{33}{}^{(n)} = F_{xy}/\delta_x \quad \text{where} \quad F_{xy} = 2\int_0^{R/2} \tau_{xy}(x)dx. \tag{3c}$$

For $n=0$, the stiffness matrix trivially coincides with that of the host.

Once the three independent coefficients $H_{lm}{}^{(n)}$ (in the following the superscript (n) will be omitted when possible, for the sake of simplicity) are known, the elastic response of the structure can be described in terms of the effective Young's modulus E, Poisson's ratio υ and coefficient of anisotropy α:

$$E = H_{11} - \frac{H_{12}{}^2}{H_{11}}, \tag{4a}$$

$$\upsilon = \frac{H_{12}}{H_{11}}, \tag{4b}$$

$$\alpha = \frac{H_{11} - H_{12}}{2H_{33}}. \tag{4c}$$

The physical meaning of E and υ is well known; the coefficient of anisotropy α determines the deviation of the shear modulus related to a square-symmetric anisotropic material from that related to isotropic media ($\alpha=1$ in the isotropic case).

In the present analysis, in order to limit the number of different cases considered, the relationship between inclusion and host phases will be described by the following condition on the stiffness matrices:

TABLE I. Dimensionless effective elastic modulus $H_{11}^{(n)}/E_h$ $(n=1,2,3,4)$ of a Sierpinski carpet $(k=\mp 9,\ \upsilon_i=\upsilon_h=0.2)$ evaluated by decreasing the size of each FE by a factor N.

$H_{11}^{(n)}/E_h$		$N=1$	$N=3$	$N=6$	$N=9$	$N=12$	$N=15$	$N=18$
$n=1$	$k=-9$	0.7839	0.7718	0.7683	0.7671	0.7666	0.7663	0.7663
	$k=+9$	1.270	1.282	1.279	1.279	1.279	1.279	1.279
$n=2$	$k=-9$	0.5905	0.5772	0.5741	0.5732	0.5728	0.5728	0.5728
	$k=+9$	1.551	1.563	1.559	1.558	1.558	1.558	1.558
$n=3$	$k=-9$	0.4442	0.4307	0.4284	0.4280	0.4280	0.4280	0.4280
	$k=+9$	1.886	1.900	1.896	1.896	1.896	1.896	1.896
$n=4$	$k=-9$	0.3291	0.2880					
	$k=+9$	2.291	2.306					

$$[H]_i = 10^k [H]_h, \tag{5}$$

where the subscripts i and h stand for inclusions and host, respectively, and k can assume integer values: negative if the inclusions are softer than the host, positive if stiffer. The choice of assuming the constant of proportionality equal to 10^k, in analogy with what performed in many other works [2,6,10,43], lets to investigate a large variety of stiffness contrasts as k varies, and it reveals useful to analyze the power laws generally expected when dealing with fractal patterns [20]. Equation (5) implies that the same relationship holds for the Young's moduli of the two phases, $E_i=10^k E_h$, while the Poisson's coefficient is the same, $\upsilon_i=\upsilon_h$. Note that a similar Poisson's ratio for the constituting phases of many composite materials is observed, such as, for instance, steel-fiber reinforced concrete ($\upsilon_i=0.2-0.3$ and $\upsilon_h=0.28$), or SiC whisker-reinforced alumina ($\upsilon_i=0.23$ and $\upsilon_h=0.17$).

A. Finite element analysis

The stress field to be inserted in Eqs. (3a)–(3c) can be computed numerically, through a FE analysis [43]. By assuming square finite elements, the size of each FE is taken equal to R_n/N, $R_n=R/3^n$, and N being the dimension of the smallest inclusion at level n and an integer number, respectively. Stresses are obtained starting from the nodal displacements evaluated, in each FE, by means of quadratic interpolation. The convergence of the numerical method is studied by increasing N: results are presented in Table I to what concerns the dimensionless component H_{11}/E_h related to the first four iterations of a Sierpinski carpet, with $k=\mp 9$ and $\upsilon_i=\upsilon_h=0.2$. Four significant digits are taken into account.

As it can be seen, the convergence is achieved for $n=1$, 2, and 3 when N reaches 15, 12, and 9, respectively. On the other hand, for $n=4$ it is not possible, from a computational point of view to refine the mesh above $N=3$. Moreover, if $n>4$, the computational effort of the procedure becomes untenable even by taking the size of each FE equal to that of the smallest inclusion R_n.

B. Position space renormalization-group technique

In order to investigate the behavior for higher-order iterations, it is possible to couple the FE analysis with the PSRG technique. This method, originally applied to problems of the conductivity [36] and of the elastic moduli of a percolation cluster [25,30], was adapted in [43] for continuous fractal structures. According to the PSRG technique, the effective elastic moduli $H_{lm}^{(n)}$, $1\le n\le 3$, of the carpet are initially evaluated [Fig. 2(a)]. This determines a mapping $f^{(n)}$: $[H]^{(0)}\to[H]^{(n)}$. The generation n, according to the terminology adopted in [39], is called a *structural cell* of the nth order. The evaluated moduli $H_{lm}^{(n)}$ are used for the renormalized host of the carpet having the same level of generation. Then the procedure is reiterated:

$$[H]^{(0)} \xrightarrow{f^{(n)}} [H]^{(n)} \xrightarrow{f^{(n)}} [H]^{(2n)} \xrightarrow{f^{(n)}} [H]^{(3n)} \xrightarrow{f^{(n)}} \cdots . \tag{6}$$

The PSRG technique is illustrated in Fig. 2(b), according to a structural cell of the first order: since at each level n the structure is composed by eight small-scaled structures of the preceding level $n-1$, the stiffness matrix of the material at the iteration $n-1$ is exploited to model the elastic behavior of the small-scaled structures at the subsequent iteration n.

Let us now compare the three independent coefficients $H_{lm}^{(n)}$ related to the first four iterations of the Sierpinski carpet ($\upsilon_i=\upsilon_h=0.2$ and $k=\mp 9$) evaluated both directly by a FE analysis and by a FE analysis coupled with a PSRG technique (Fig. 3). A structural cell of the first order is implemented. As can be seen, results are in good agreement apart from $n=4$, as expected due to the computational problem presented above. Observe the nonlinear behavior of the curves, especially that related to softer inclusions, which leads to a different scaling for the coefficients $H_{lm}^{(n)}$ in the first generations of the structure [41]. Further details on the accuracy of the PSRG technique and on the equivalence of the results obtained through different order cells can be found in [43].

Before proceeding, let us denote with L the characteristic length of the Sierpinski carpet, defined as the ratio between the largest side of the carpet R and the smallest inclusion dimension R_n, $L=R/R_n=3^n$. The inclusion area fraction ρ can be expressed, through L, as

$$\rho = 1 - \left(\frac{R_n}{R}\right)^{2-D} = 1 - L^{D-2}, \tag{7}$$

with $D=\log_{10} 8/\log_{10} 3 \approx 1.893$ being the fractal dimension of the carpet.

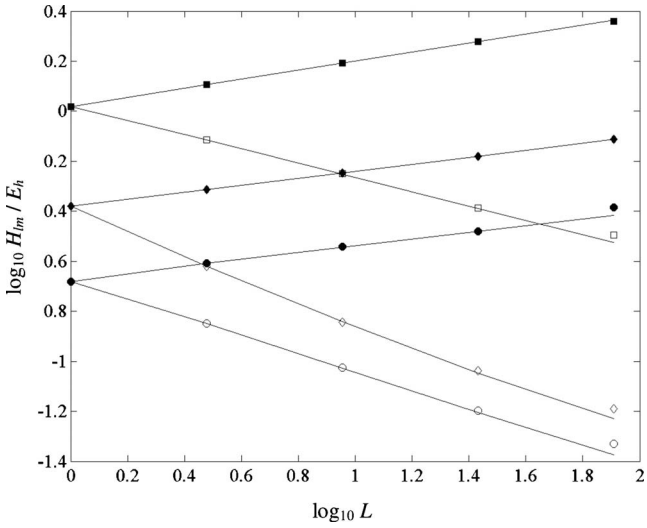

FIG. 3. Dimensionless effective elastic moduli of a Sierpinski carpet, with $\upsilon_i=\upsilon_h=0.2$ and $k=\mp 9$, vs dimensionless size L for the first four iterations. The moduli referring to $k=-9$ and obtained directly by a FE analysis are indicated by empty squares (H_{11}), by circles (H_{12}), and by diamonds (H_{33}). The filled marks denote the corresponding moduli for $k=+9$. The lines represent the results obtained by means of the PSRG technique with a first-order structural cell.

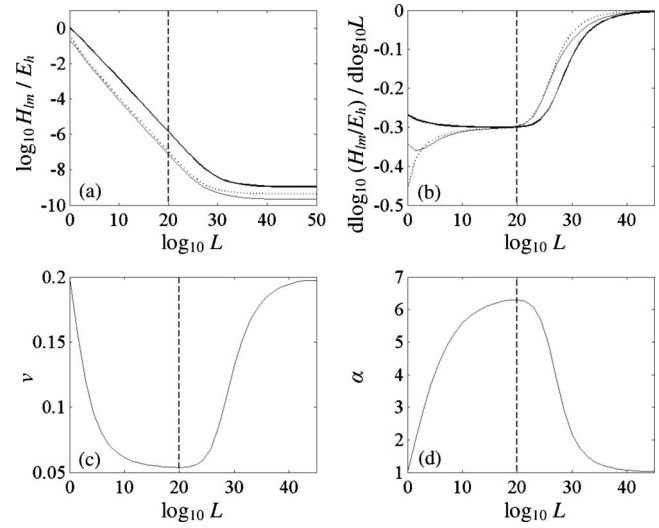

FIG. 4. (a) Dimensionless effective elastic moduli, (b) logarithmic derivatives, (c) Poisson's ratio υ, and (d) coefficient of anisotropy α of a Sierpinski carpet ($k=-9$ and $\upsilon_i=\upsilon_h=0.2$) vs dimensionless size L. The vertical dashed line denotes the logarithmic value of the critical threshold L_c. In (a) and (b) the thick continuous line refers to H_{11}, the thin continuous line refers to H_{12} and the dotted line refers to H_{33}.

III. RESULTS AND DISCUSSION

In [43] only the cases of voids and rigid particles were considered by assuming $k=\mp 9$ in Eq. (5). The coefficients of the elastic matrix are found to possess, for large n, the same scaling:

$$H_{lm}^{(n)} = H_{lm}^{(0)} L^s \tag{8}$$

being $[H]^{(0)}=[H]_h$ and where $s=-0.284$ for the porous carpet ($k=-9$) and $s=+0.168$ for rigid inclusions ($k=9$), respectively. Consequently, according to Eqs. (4b) and (4c), both the Poisson's and the anisotropy coefficients tend to a constant value and a fixed point $(\bar{\upsilon},\bar{\alpha})$ in the υ-α flow diagram is detected for sufficiently high-order n.

A first important consideration in the present analysis can be made by observing Fig. 4. The logarithmic dependence of the three elastic moduli on the dimensionless size of the carpet ($k=-9$ and $\upsilon_i=\upsilon_h=0.2$) is reported in Fig. 4(a), and the behavior of the their logarithmic derivatives with respect to $\log_{10} L$ is plotted in Fig. 4(b). The graphs are obtained through a third-order structural cell.

While the elastic modulus scaling is initially different, as n increases ($\log_{10} L>15$) all the curves show the same slopes, the difference between each other being less than 1%. This behavior is observed until a specific iteration n_c ($\log_{10} L\approx 20$), indicated by the dashed line in Fig. 4, which will be called, hereafter, *critical threshold* as well as the related quantities, L_c and ρ_c. In correspondence with n_c, both the υ and α curves present a stationarity point, a minimum [Fig. 4(c)] and a maximum [Fig. 4(d)], respectively. Then, the slope of H_{11} starts to deviate from that related to the other two coefficients. The three curves show again the same scaling (zero) only for sufficiently large n ($\log_{10} L>40$) when the elastic moduli approach those of the inclusions.

As pointed in [6], there always exists a qualitative distinction between very soft inclusions and vacuous pores. In order to investigate the convergence to the case of pores, different computations with different stiffness contrasts ($k=-3,-6,-9,-\infty$) between the phases have been performed. If the condition $k=-\infty$ is imposed in Eq. (6), a meaningless oscillatory behavior is observed in the H_{lm} curves and consequently for the effective elastic characteristics E, υ (Fig. 5) and α [Eqs. (4a)–(4c)]. As a matter of fact, if the effective elastic moduli H_{lm} of the composite asymptotically tend to zero according to Eq. (6), the corresponding limits for the effective elastic characteristics E, υ, and α,

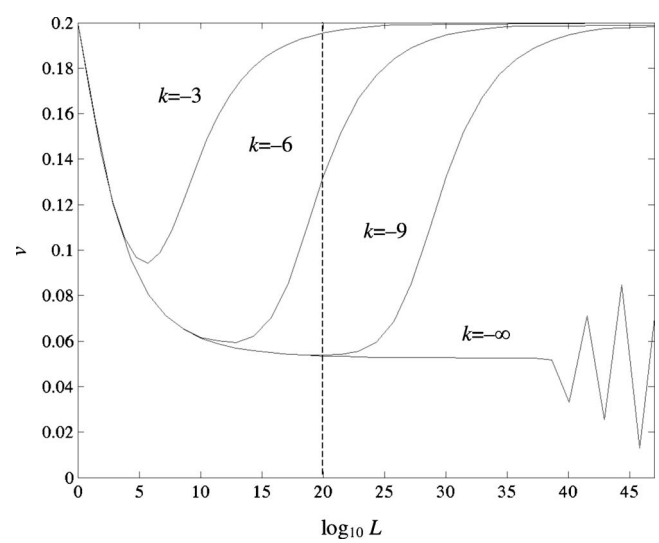

FIG. 5. Effective Poisson's ratio of a Sierpinski carpet vs dimensionless size L for different negative values of k.

TABLE II. Exponent s governing the power law of the Young's modulus E and critical iterations n_c for a Sierpinski carpet with $\upsilon_i = \upsilon_h = 0.2$. Negative or positive values of k correspond to soft or stiff inclusions, respectively.

k	−1	−2	−3	−4	−5	−9
s	−0.1871	−0.2652	−0.2757	−0.2819	−0.2872	−0.2913
n_c	5	8	12	17	22	44
k	+1	+2	+3	+4	+5	+9
s	+0.1388	+0.1672	+0.1726	+0.1730	+0.1732	+0.1733
n_c	9	14	21	30	39	78

result to be undetermined. On the other hand, the condition $k=-9$ represents a good approximation to the porous case (Fig. 5): the difference between the two Poisson's ratios evaluated at n_c and just before the oscillating behavior is less than 1%

Analogous considerations hold between rigid and extremely rigid inclusions.

In what follows, the effective elastic properties of these fractal-like composites, in terms of E, υ, and α, are investigated for different values of $|k|$, ranging from 1 to 9, and for different Poisson's ratios, $\upsilon_i=\upsilon_h=0.1,0.2,0.3,0.4$. Both host and inclusions are always supposed to be isotropic, i.e., $\alpha_i=\alpha_h=1$. Structural cells of the first, second, and third order are exploited for $|k|=1,2$, for $|k|=3,4,5$ and for $|k|=9$, respectively. Notice that, for $|k|<9$, n_c simply identifies the stationarity points on the υ and α vs $L(\rho)$ curves.

A. Young's modulus

The effective Young's modulus E [Eq. (4a)] of a Sierpinski-like composite satisfies the following power law until the critical threshold L_c [Fig. 5(b)]:

$$E = E^{(0)} L^s, \tag{9}$$

where $E^{(0)}=E_h$, in perfect analogy with Eq. (8). The validity of Eq. (9) can be assumed, without loosing of generality, in the full range $0<L\leq L_c$, since E is strongly dependent on H_{11} and the scaling of H_{11} does not show large deviations until the iteration n_c [Fig. 4(b)]. According to Eq. (9), a linear behavior is observed in a double logarithmic scale: the values of the slope s are reported in Table II when $\upsilon_i=\upsilon_h=0.2$, for both soft and stiff inclusions. As $|k|$ increases, s converges: the limit is higher, in absolute value, for soft inclusions. The ratio between these limits is approximately equal to 1.682. In the case of isotropic media filled by circular inclusions, the limit ratio is exactly 2 [21]. This difference is imputable to the different inclusion shape, which, in the present case, leads to the anisotropic behavior described in Sec. III C. On the other hand, the small deviation from the results presented in [43] may be due to a different mesh adopted. Eventually, note that, for soft inclusions, the exponents s do not coincide with the quantity $2-D\approx 0.107$, providing classical mixture rules [see Eq. (7) [22]].

In Table II there are also indicated the values of the critical iteration n_c. Although they are approximated, since the small scattering observed between nearest iterations in most of the cases, it can be evinced that, for soft inclusions, n_c always occurs before by a factor ranging from 1.750 to 1.800.

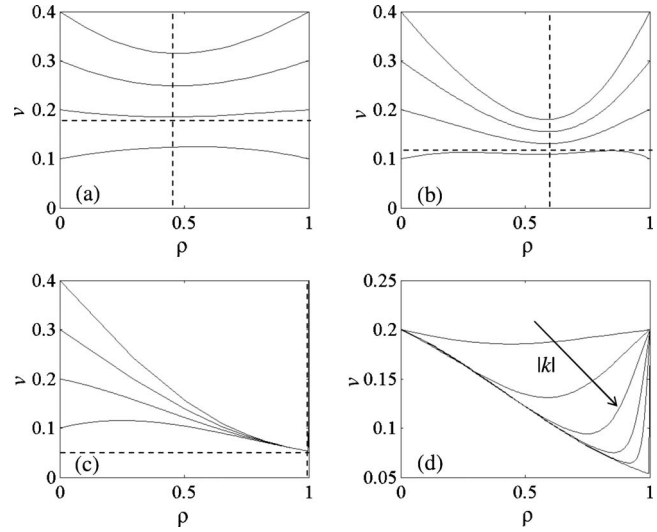

FIG. 6. Poisson's ratio υ vs inclusion area fraction ρ, for soft inclusions: (a) $k=-1$, (b) $k=-2$, and (c) $k=-9$. The vertical and horizontal dashed lines represent the critical threshold ρ_c and the fixed point υ^*, respectively. In (d) results related to the case $\upsilon_i=\upsilon_h=0.2$, for $k=-1,-2,-3,-4,-5,-9$, are reported.

Exponents s and critical iterations n_c related to different values of $\upsilon_i=\upsilon_h$ slightly vary as long as $|k|\leq 3$, while they coincide for higher $|k|$. It can hence be deduced that the Young's modulus E of a fractal biphase composite material, for sufficiently high ratios E_i/E_h, is totally independent of the Poisson ratio's of the host υ_h. This result is in good agreement with those presented in the paper [10]. For $n\rightarrow\infty$, the Young's modulus of the composite approaches that of the inclusions.

B. Poisson's ratio

The FE analysis coupled with the PSRG technique is now used to describe how the effective Poisson's ratio υ [Eq. (4b)], as a function of the inclusion area fraction ρ, depends on $\upsilon_i=\upsilon_h$ and E_i/E_h [i.e., k, Eq. (5)]. The results are plotted in Figs. 6 and 7 for what concerns soft or stiff inclusions, respectively. Obviously, for $\rho=0$, only the matrix is present, while $\rho=1$ corresponds to the inclusion material: thus, all the curves start and end at the same points $\upsilon_i=\upsilon_h$.

First of all, it is worthwhile observing that, since generally υ is not bounded between the Poisson's ratio of the matrix and inclusion phases, no mixing rules hold true. On the other hand, there always exists a critical value $\upsilon=\upsilon^*$ which is independent of ρ, unless some negligible scatterings. The critical value υ^* is indicated by the horizontal dashed line in Figs. 4 and 5. For low $|k|$ [Figs. 4, 5(a), and 5(b)], when $\upsilon_i=\upsilon_h<\upsilon^*$, the effective Poisson's ratio is always less than υ^* and greater than $\upsilon_i=\upsilon_h$, with a maximum value. On the other hand, when $\upsilon_i=\upsilon_h>\upsilon^*$, the effective Poisson's ratio is always higher than υ^* and less than

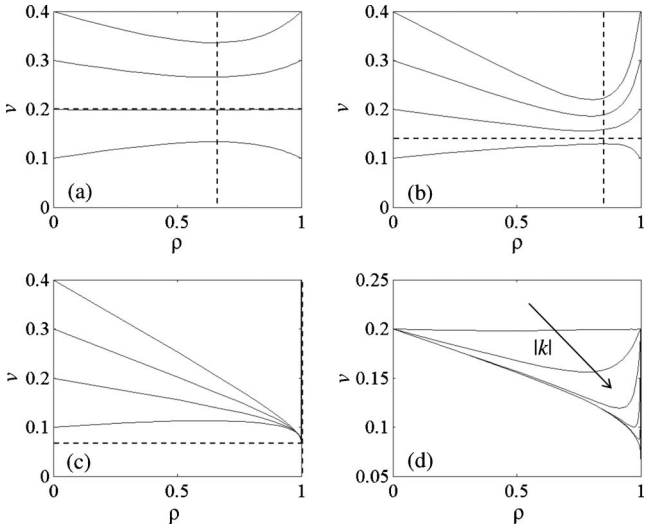

FIG. 7. Poisson's ratio υ vs inclusion area fraction ρ for stiff inclusions: (a) $k=1$, (b) $k=2$, and (c) $k=9$. The vertical and horizontal dashed lines represent the critical threshold ρ_c and the fixed point υ^*, respectively. In (d) results related to the case $\upsilon_i=\upsilon_h=0.2$, for $k=1,2,3,4,5,9$, are reported.

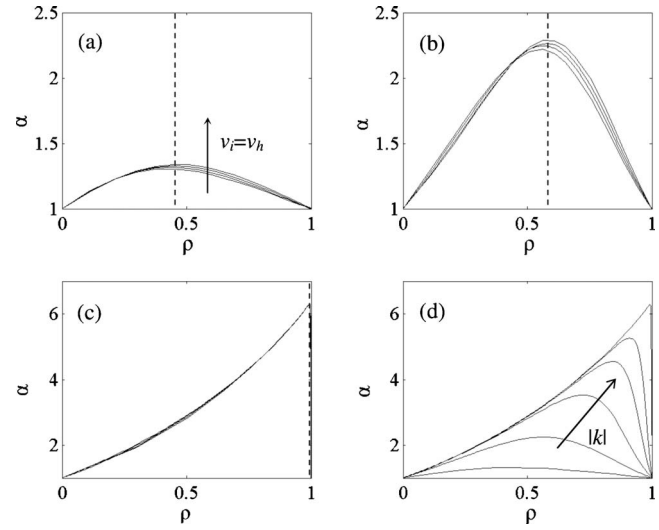

FIG. 8. Coefficient of anisotropy α vs inclusion area fraction ρ, for soft inclusions: (a) $k=-1$, (b) $k=-2$, and (c) $k=-9$. The vertical dashed line represents the critical threshold ρ_c. In (d) results related to the case $\upsilon_i=\upsilon_h=0.2$, for $k=-1,-2,-3,-4,-5,-9$, are reported.

$\upsilon_i=\upsilon_h$, with a minimum value. The stationary points, in the υ-ρ plane, are attained in correspondence with the critical threshold ρ_c, denoted by the vertical dashed line, and depend on the elastic stiffness mismatch between the phases E_i/E_h. Also the critical value υ^* depends on E_i/E_h, differently from what found for isotropic composites with circular inclusions [1–6]. On the other hand, a similar trend also emerges in [44], showing that media with fractal structure have properties which are different from those of ordinary composites. As $|k|$ increases, ρ_c tends to unity and υ^* decreases. This is again probably due to the anisotropy induced by the structure geometry, which becomes more marked as $|k|$ increases. Note that the results related to soft or stiff inclusions differ from each other [Figs. 4 and 5(d)] for equal $|k|$: in the former case the critical threshold is attained before and υ^* is lower. However, the ratio between the two values of υ^* nearly remains constant for the same $|k|$.

In addition to the critical point behavior, in the limit cases of $k=\mp 9$ [Figs. 6 and 7(c)], all the curves meet each other at the fixed point $\bar{\upsilon}=\upsilon^*$ at ρ_c, which is very close to 1. As well explained in [10] for porous media, this implies that the shape of the solid host dominates the lateral expansion under uniaxial compression rather than the material properties. For the structure under examination, it is found that $\bar{\upsilon}=0.0547$ or 0.0671 for soft or stiff inclusions, respectively. Slightly different results were obtained in [43], $\bar{\upsilon}\approx 0.063$ and $\bar{\upsilon}\approx 0.065$.

C. Coefficient of anisotropy

As discussed in the previous sections, both the phases are considered to be isotropic ($\alpha_i=\alpha_h=1$). Therefore, all the α-ρ curves in Figs. 8 and 9 start and end at $\alpha=1$ since $\rho=0$ represents the matrix and $\rho=1$ represents the inclusion material. In spite of this, the global behavior becomes anisotropic for the intermediate cases $0<\rho<1$, with $\alpha>1$, denoting a reduction in the shear modulus with respect to the isotropic case [Eq. (4c)]. Thus, again, no mixture law keeps true. The maximum is reached in correspondence with ρ_c and it increases, as well as ρ_c, for increasing $|k|$. Eventually, for $k=\mp 9$ all the α-ρ curves meet each other at a fixed point $\bar{\alpha}$, irrespective of the host elastic properties, which is estimated to be $\bar{\alpha}=6.252$ for soft inclusions and $\bar{\alpha}=4.453$ for stiff inclusions. Note that the anisotropy is more pronounced for soft inclusions. A similar behavior is also detected from the analysis on anisotropic elastic and superelastic percolation networks [28].

Whether $\bar{\alpha}$ is connected with $\bar{\upsilon}$ and which is the relationship between these two quantities is still object of investiga-

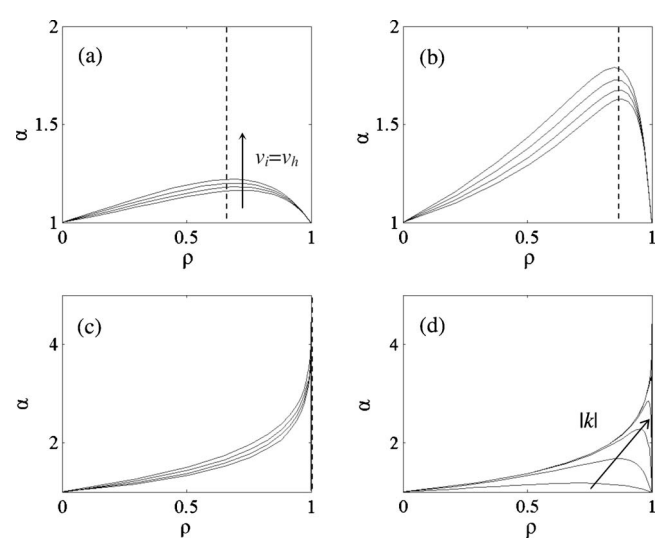

FIG. 9. Coefficient of anisotropy α vs inclusion area fraction ρ for stiff inclusions: (a) $k=1$, (b) $k=2$, (c) and $k=9$. The vertical dashed line represents the critical threshold ρ_c. In (d) results related to the case $\upsilon_i=\upsilon_h=0.2$, for $k=1,2,3,4,5,9$, are reported.

tion. One idea could be that of extending the formulas derived for isotropic composite materials with circular inclusion, by properly introducing the anisotropy α. For instance, it could be hypothesized that $\bar{v}=1/[\bar{\alpha}(2d-1)]$ (with $d=2$), which provides good results for soft inclusions. Although this applies also for data related to other fractal structures [43], it could simply be a fortunate coincidence. Deeper studies may concern also the different behavior observed for stiff and soft inclusions. Finally, in the framework of future developments, it might be interesting to generalize the analysis to the three-dimensional case, to see how these inherently two-dimensional results can be extended. In fact, up to now, only the work by Poutet *et al.* [42] is available in the paper and is only limited to the first three fractal iterations.

IV. CONCLUSIONS

In this work it is shown that no mixture rules hold for the effective elastic properties of fractal-like composites. Both the Poisson's ratio v and the coefficient of anisotropy α present some stationarity points, whose values, as well as the critical iteration at which they are attained, depend on the elastic stiffness mismatch between the phases. Eventually, in the cases of pores or absolutely rigid inclusions, these points become fixed: thus, the effective elastic properties of a well-developed Sierpinski carpet result to be independent of the host elastic moduli [43]. The comparison with the results obtained for generic composite materials shows some analogies and suggests some interesting future developments.

ACKNOWLEDGMENTS

The financial support of the Italian Ministry of Education, University and Research (MIUR) to the Project "Advanced applications of Fracture Mechanics for the study of integrity and durability of materials and structures" within the "Programmi di Ricerca Scientifica di Rilevante Interesse Nazionale (PRIN)" program is gratefully acknowledged.

[1] A. R. Day, K. A. Snyder, E. J. Garboczi, and M. F. Thorpe, J. Mech. Phys. Solids **40**, 1031 (1992).
[2] K. A. Snyder, E. J. Garboczi, and A. R. Day, J. Appl. Phys. **72**, 5948 (1992).
[3] E. J. Garboczi and A. R. Day, J. Mech. Phys. Solids **43**, 1349 (1995).
[4] A. Cherkaev, K. Lurie, and G. W. Milton, Proc. R. Soc. London, Ser. A **438**, 519 (1992).
[5] M. F. Thorpe and I. Jasiuk, Proc. R. Soc. London, Ser. A **438**, 531 (1992).
[6] R. W. Zimmerman, Appl. Mech. Rev. **47**, S38 (1994).
[7] T. Mori and K. Tamaka, Acta Metall. **21**, 571 (1973).
[8] Z. Hashin, Trans. ASME, J. Appl. Mech. **50**, 481 (1983).
[9] S. Torquato, Appl. Mech. Rev. **44**, 37 (1991).
[10] A. P. Roberts and E. J. Garboczi, Proc. R. Soc. London, Ser. A **458**, 1033 (2002).
[11] S. Vigdergauz, Math. Mech. Solids **12**, 58 (2007).
[12] R. M. Christensen, Proc. R. Soc. London, Ser. A **440**, 461 (1993).
[13] R. W. Zimmerman, J. Mater. Sci. Lett. **4**, 1457 (1985).
[14] L. M. Schwartz, S. Feng, M. F. Thorpe, and P. N. Seng, Phys. Rev. B **32**, 4607 (1985).
[15] A. N. Norris, Int. J. Solids Struct. **26**, 663 (1990).
[16] S. Meille and E. J. Garboczi, Modell. Simul. Mater. Sci. Eng. **9**, 371 (2001).
[17] R. Lakes, Nature (London) **361**, 511 (1993).
[18] H. J. Brown and G. B. West, *Scaling in Biology* (Oxford University Press, Oxford, 1999).
[19] A. S. Balankin, Phys. Rev. B **53**, 5438 (1996).
[20] A. Carpinteri and N. Pugno, Nature Mater. **4**, 421 (2005).
[21] A. V. Dyskin, Int. J. Solids Struct. **42**, 477 (2005).
[22] N. Pugno and A. Carpinteri, Philos. Mag. Lett. **88**, 397 (2008).
[23] S. Feng and P. N. Sen, Phys. Rev. Lett. **52**, 216 (1984).
[24] Y. Kantor and I. Webman, Phys. Rev. Lett. **52**, 1891 (1984).
[25] S. Feng and M. Sahimi, Phys. Rev. B **31**, 1671 (1985).
[26] M. Sahimi and J. D. Goddard, Phys. Rev. B **33**, 7848 (1986).
[27] E. Duering and D. J. Bergman, Phys. Rev. B **37**, 9460 (1988).
[28] L. Limat, Phys. Rev. B **40**, 9253 (1989).
[29] M. Sahimi and S. Arbabi, Phys. Rev. Lett. **68**, 608 (1992).
[30] M. A. Knackstedt and M. Sahimi, J. Stat. Phys. **69**, 887 (1992).
[31] S. Arbabi and M. Sahimi, Phys. Rev. B **47**, 695 (1993).
[32] M. Sahimi and S. Arbabi, Phys. Rev. B **47**, 703 (1993); **47**, 713 (1993).
[33] M. Sahimi, Phys. Rep. **306**, 213 (1998).
[34] D. J. Bergman and Y. Kantor, Phys. Rev. Lett. **53**, 511 (1984).
[35] M. Epstein and S. Adeeb, Int. J. Solids Struct. **45**, 3238 (2008).
[36] J. Bernasconi, Phys. Rev. B **18**, 2185 (1978).
[37] D. J. Bergman and D. G. Stroud, Phys. Rev. B **62**, 6603 (2000).
[38] M. Latva-Kokko, J. Mäkinen, and J. Timonen, Phys. Rev. E **63**, 046113 (2001).
[39] M. Latva-Kokko and J. Timonen, Phys. Rev. E **64**, 066117 (2001).
[40] D. A. Head, F. C. MacKintosh, and A. J. Levine, Phys. Rev. E **68**, 025101 (2003).
[41] P. Sheng and R. Tao, Phys. Rev. B **31**, 6131 (1985).
[42] J. Poutet, D. Manzoni, F. Hage-Chehade, C. J. Jackin, M. J. Boutéca, J.-F- Thovert and P. M. Adler, J. Mech. Phys. Solids **44**, 1587 (1996).
[43] V. G. Oshmyan, S. A. Patlazhan, and S. A. Timan, Phys. Rev. E **64**, 056108 (2001).
[44] V. V. Novikov, K. W. Wojciechowski, D. V. Belov, and V. P. Privalko, Phys. Rev. E **63**, 036120 (2001).
[45] V. V. Novikov and D. Y. Zubkov, Phys. Rev. B **73**, 054202 (2006).